IMPORTANCE OF THE COLLISIONAL BROADENING OF THE STATES ACROSS MOSFET TECHNOLOGY GENERATIONS

Gokula Kannan
School of Electrical, Computer and Energy Engineering
Arizona State University
Tempe, AZ 85287-5706, USA
gokulaka@asu.edu

Dragica Vasileska
School of Electrical, Computer and Energy Engineering
Arizona State University
Tempe, AZ 85287-5706, USA
vasileska@asu.edu

Abstract— **There are two assumptions made in the derivation of the Fermi's Golden Rule: (1) it is assumed that the scattering is infrequent which allows us to impose the long time limit and arrive at the energy conserving delta function, and (2) collision duration time is assumed to be zero, which implies that the intra-collisional field effect is neglected. The assumption (1) basically means that collisional broadening of the states (CBS) is being ignored in many analyses of deep-submicrometer devices. But when is that assumption valid? This is the point we want to address here. For that purpose we investigate the effect of CBS on three different technologies of MOSFET devices with substrate doping densities equal to 10^{17}cm^{-3}, 5×10^{17}cm^{-3}, and 10^{18}cm^{-3}.**

Keywords: scattering, collisional broadening of the states, DOS function

I. INTRODUCTION

It is well known that in deep submicron devices, due to high substrate doping, the transverse electric field reaches very high values which leads to significant bending of the conduction band near the Si/SiO2 interface, even near the threshold of inversion. Since the width of the confining potential in these devices becomes comparable to the thermal deBroglie wavelength of the carriers, size-effect quantization leads to widely spaced electron energy levels [1]. The resultant energy levels are grouped into electronic subbands each of which represents spatially constrained Bloch waves traveling in the plane parallel to the interface.

To describe the system more realistically such that the results obtained can reflect the experimental situation, we calculate the envelope wavefunctions and the corresponding bound-state energies along the growth direction (z-axis) by solving self-consistently the one-dimensional Poisson and Schrödinger equations, with the latter expressed in the form given by Hohenberg and Kohn [2], and Kohn and Sham [3]. In the calculation of the broadening of the states and conductivity we use the real-time Green's functions formalism due to Keldysh [4], and Kadanoff and Baym [5]. An interested reader can find a detailed description of this field-theoretical technique in the review article by Rammer and Smith [6].

Scattering induced broadening of the states, and the renormalization of the spectrum, are calculated through the solution of Dyson's equation for the retarded Green's function [7]. The scattering mechanisms included in the model are Coulomb scattering from both of the depletion layer and interface/ oxide charges, surface-roughness scattering, zero- and first-order intervalley optical phonon scattering processes, and inter-subband acoustic phonon scattering. The self-energy contributions are calculated within the self-consistent Born approximation. As already mentioned, screening of the Coulomb and surface-roughness scattering potentials is taken into account within the Random Phase Approximation (RPA). For the temperature-dependent RPA polarizability function we use the result given in Ref. [8] which is valid for general Fermi-Dirac statistics. For intervalley scattering, which is the dominant scattering mechanism in many-valley semiconductors such as Si and Ge, we follow an approach due to Price [9] and Ridley [10]. We use the same phonon energies and coupling constants in the intersubband scatterings as those in intervalley scattering in bulk silicon [11], which is shown to give excellent results for transport in silicon devices [12]. The anisotropy of the deformation potential interaction is treated as described in Refs. [13,14]. More details about the model are given below and in Ref. [15].

II. THEORETICAL MODEL AND IMPLEMENTATION DETAILS

Using the diagonal approximation for the full(dressed) Green's function, from the coupled Dyson's equations [15] we get that the Fourier transform of the retarded subband Green's function is

$$g_n^r(\mathbf{k},\omega) = \frac{1}{\hbar\omega - \varepsilon_{\mathbf{k}} - \varepsilon_n - \Sigma_n^r(\mathbf{k},\omega)} \quad . \qquad (1)$$

The retarded subband self-energy $\Sigma_n^r(\mathbf{k},\omega)$ that appears in Eq. (1) is calculated to be of the form

$$\Sigma_n^r(\mathbf{k},\omega) = \iint dz dz_1 \left[\psi_n^*(z)\Sigma_r(z,z_1,\mathbf{k},\omega)\,\psi_n(z_1)\right]. \qquad (2)$$

Since impurity and surface-roughness are independent scattering mechanisms, both of which may be assumed to be weak, we can perform the averaging processes separately. Under these circumstances, the total self-energy is calculated

as a sum of the independent contributions from each scattering mechanisms. We found that, within the self-consistent Born-approximation [15], the general form of the retarded subband self-energy for impurity and surface-roughness scattering is

$$\Sigma_n^r(\mathbf{k},\omega) = \sum_m \sum_{\mathbf{q}} \sum_i \left|U_{nm}^i(\mathbf{q})\right|^2 g_m^r(\mathbf{k}-\mathbf{q},\omega) . \quad (3)$$

The summation over i is a summation over the scattering processes that dominate the transport properties of the system under consideration. Since the retarded Green's function is always of the form

$$g_n^r(\mathbf{k},\omega) = \frac{1}{\hbar\omega - \varepsilon_{\mathbf{k}} - \varepsilon_n - R_n(\mathbf{k},\omega) + i\Gamma_n(\mathbf{k},\omega)} , \quad (4)$$

where $R_n(\mathbf{k},\omega)$ gives the shift in the subband energies, which is usually small, and $\Gamma_n(\mathbf{k},\omega)$ is proportional to the inverse of the lifetime of the n-th state (τ_n), substituting (4) into (3) leads to the following expressions

$$\Gamma_n(\mathbf{k},\omega) = \frac{1}{2}\sum_m \iint \frac{d^2q}{(2\pi)^2} a_m(\mathbf{q},\omega) \sum_i \left|U_{nm}^i(\mathbf{k}-\mathbf{q})\right|^2 , \quad (5a)$$

$$R_n(\mathrm{k},\omega) = \sum_m \iint \frac{d^2q}{(2\pi)^2} \sum_i \left|U_{nm}^i(\mathrm{k}-\mathrm{q})\right|^2 \times \times \frac{\hbar\omega - \varepsilon_{\mathrm{q}} - \varepsilon_m - R_m(\mathrm{q},\omega)}{\left[\hbar\omega - \varepsilon_{\mathrm{q}} - \varepsilon_m - R_m(\mathrm{q},\omega)\right]^2 + \Gamma_m^2(\mathrm{q},\omega)} , \quad (5b)$$

for the broadening of the electronic states of the n-th subband and the energy renormalization term $R_n(\mathbf{k},\omega)$, respectively, where $a_n(\mathbf{q},\omega) = -2\,\mathrm{Im}\left\{g_n^r(\mathbf{q},\omega)\right\}$ is the spectral density function. From the results given in Eq. (5) it is clear that the interacting Green's function must be found self-consistently, because the various subbands are explicitly linked through the self-energy terms. The DOS function is then calculated as a summation over the momentum states of the spectral density function.

Calculation of the retarded self-energy for electron-phonon interactions is more complicated and it is based on several approximations. First, we assume that the reservoir (phonon bath) is in thermal equilibrium and we will restrict ourselves to one-phonon processes as one does in deriving the Fermi's golden rule. In the self-consistent Born approximation, the self-energy function due to electron-phonon interaction graphically shown in Fig. 1, is given by [16]

$$\Sigma^{<,>}(x_1,x_2) = iG^{<,>}(x_1,x_2)D^{<,>}(x_1,x_2) , \quad (6)$$

where $D^{<,>}$ are the phonon Green's functions. Then, the retarded/advanced self-energy functions for the electron-phonon interaction are given by

$$\Sigma_{r/a}(x_1,x_2) = iG_{r/a}(x_1,x_2)D^{>}(x_1,x_2) + +iG^{<}(x_1,x_2)D_{r/a}(x_1,x_2) . \quad (7)$$

For reasonably small electron densities, the term containing $G^{<}$ is a negligible correction to the term containing G_r. With this approximation, the result for the retarded/advanced self-energy functions simplifies to

$$\Sigma_{r/a}(x_1,x_2) = iG_{r/a}(x_1,x_2)D^{>}(x_1,x_2) . \quad (8)$$

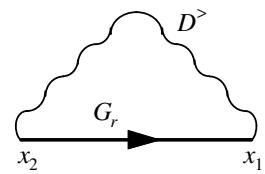

Fig. 1.Self-consistent Born approximation for electron-phonon interaction.

This approximation also decouples the Dyson equation for G_r from the Keldysh equation for $G^{<}$ [4]. Furthermore, if one assumes that the electrons do not influence the phonon states, the phonons can be treated as being in equilibrium. Substituting the result for greater-than phonon Green's function given in (8) into (7), and using the diagonal approximation for the retarded Green's function, we find that the self-energy defined in Eq. (8) reduces to

$$\Sigma_n^r(\mathrm{k},\omega) = \sum_m \sum_{\mathrm{q}} \sum_i \left|U_{\lambda,nm}^i(\mathrm{q})\right|^2 \begin{bmatrix} \left(N_{\mathrm{Q}\lambda}+1\right) g_n^r\left(\mathrm{k}-\mathrm{q},\omega-\omega_{\mathrm{q}\lambda}\right) + \\ N_{\mathrm{Q}\lambda} g_n^r\left(\mathrm{k}-\mathrm{q},\omega+\omega_{\mathrm{q}\lambda}\right) \end{bmatrix} . \quad (9)$$

The first term inside the brackets of Eq. (9) corresponds to the phonon emission and the second one to the phonon absorption process. Again, the total self-energy equals to the sum of the contributions from different electron-phonon interactions. The expressions for the broadening of the electronic states $\Gamma_n(\mathbf{k},\omega)$ and the renormalization factor $R_n(\mathbf{k},\omega)$ for the subband energies are identical to the ones given in Eq. (5) for this case too. The only difference is that, instead of having one, we now have two terms on the RHS of Eq. (9) that are shifted in frequency. In the elastic approximation valid for acoustic phonons, these frequency shifts are ignored since the energy of the acoustic phonons is usually much smaller than the thermal energy of the electrons.

III. Simulation Results

Once the collisional broadening of the states and the renormalizations of the spectrum are calculated according to the results given in Eq. (5), the density of states function

(DOS) is calculated by integrating the spectral density function, according to equation

$$\rho_0(\omega) = \frac{1}{\pi}\sum_{n,k} a_{0n}(k,\omega) \ . \qquad (10)$$

Then, the importance of various scattering mechanisms is deducted via examination of the shape of the density of states function, which in an ideal case approaches a step function. The results of these investigations are presented in Fig. 2.

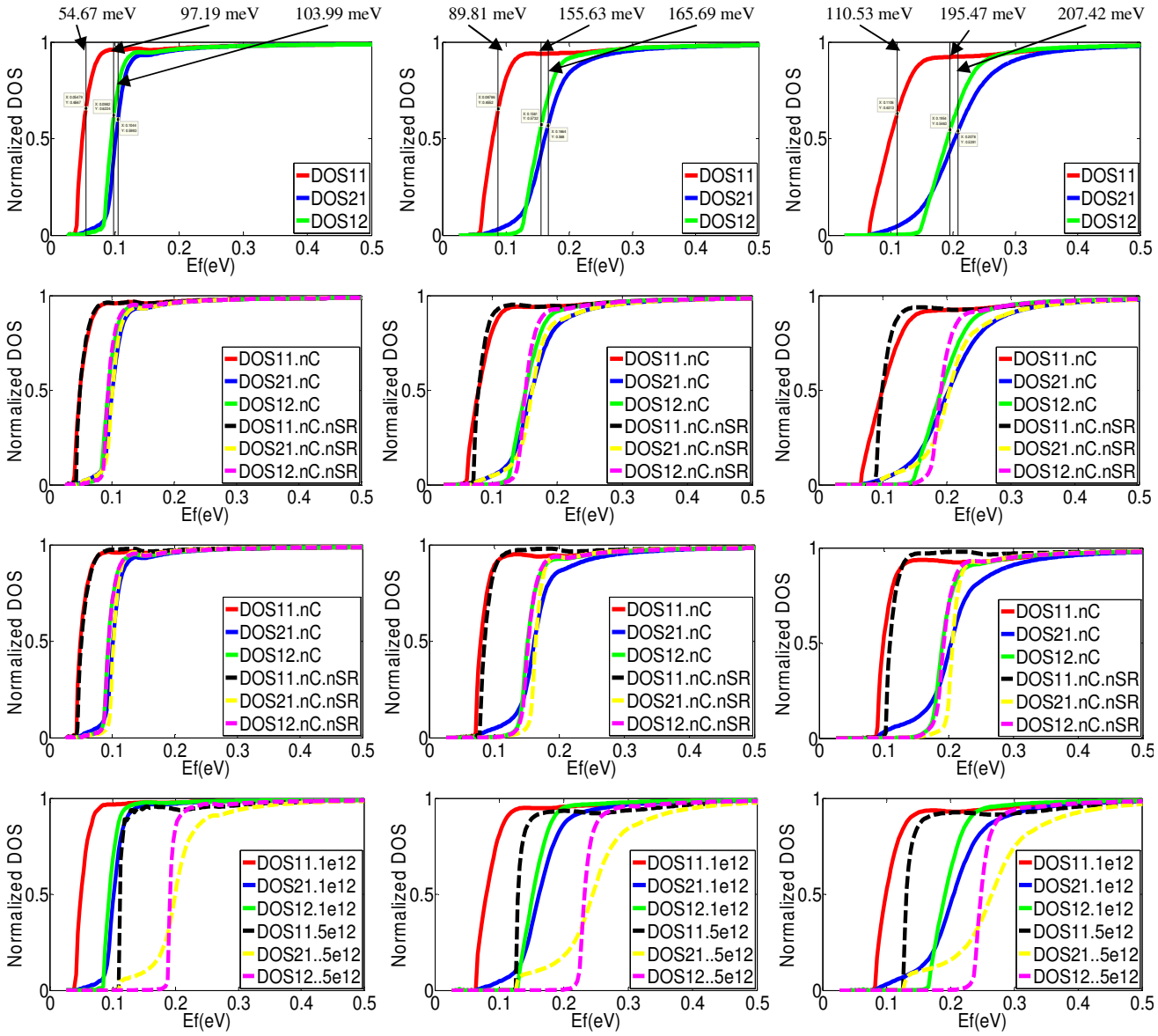

Fig.2. Left panel $N_A = 10^{17}cm^{-3}$, Middle panel $N_A = 5\times10^{17}cm^{-3}$, Right panel $N_A = 10^{18}cm^{-3}$.First row panels: Effective (real) DOS of the lowest three subbands (2 from unprimed ladder of subbands (11 and 21) and 1 from primed ladder of subbands (12)). Renormalization of the spectrum is not taken into account. Sheet electron density is 10^{12} cm $^{-3}$. The energy values indicate the corresponding subband energies in the order of subbands – 11, 12, 21. Second Row panels: Simulation run without Coulomb scattering. "DOS.nC" denotes the real DOS function without Coulomb scattering in comparison to the real DOS with Coulomb scattering denoted by "DOS". Third Row panels: Simulation run without Coulomb scattering and without surface roughness scattering. "DOS.nC.nSR" denotes the real DOS function without Coulomb scattering and surface roughness scattering in comparison to the real DOS without Coulomb scattering only denoted by "DOS.nC". Fourth Row panel: Simulation run with all scattering mechanisms included for 2 sheet charge densities, "DOS.1e12" – sheet charge density of $1\times10^{12}cm^{-2}$, "DOS.5e12" – sheet charge density of $5\times10^{12}cm^{-2}$.

IV. Discussion of the Results

The left panels of Fig. 2 describe the DOS results corresponding to substrate doping density of 10^{17} cm^{-3}, the middle panels to substrate doping density of 5×10^{17} cm^{-3} and the right panel to substrate doping density of 10^{18} cm^{-3}. The first panel corresponds to the case when all scattering mechanisms are incorporated in the model. The subband energies for the respective subbands are also indicated. The lines denote the ideal DOS step-function. We can observe that the broadening of the states induced by the scattering leads to the spreading of the DOS function around this energy value for a given subband.

The second panel results correspond to a case when Coulomb scattering is omitted and the third panel results correspond to the case when both Coulomb and surface roughness scattering are not included in the theoretical model. One can immediately conclude by the comparison of the results for the DOS function that for the case of substrate doping density of 10^{17} cm^{-3} Coulomb and surface-roughness scattering are not that significant when compared to phonon scattering as the DOS function shape does not change significantly. The situation is similar for the substrate doping density of 5×10^{17} cm^{-3} because although both Coulomb and interface roughness scattering potentials are higher, the subband separation increases and the intersubband scattering reduces due to the smaller overlap of the wavefunctions; thus leading to smaller overlap factors.

The situation is a little different for substrate doping density of 10^{18} cm^{-3}. Here, although the subband separation is higher, the strength of both Coulomb and surface-roughness potentials increases considerably, thus dominating phonon scattering even at sheet electron density of 10^{12} cm^{-2}. Such orders of doping density roughly corresponds to substrate doping density of 32 nm and 22 nm technology nodes.

In the bottom panel, we have a plot of the DOS function for two sheet charge densities 1×10^{12} cm^{-2} and 5×10^{12} cm^{-2}. It can be observed that as the sheet density increases, the subband energies and their separation increase as well which leads to larger energy shift between the DOS function corresponding to the different subbands. Also noted is that the second subband of the first valley has the highest broadening. This can be explained by looking at the second and third panel for the 1×10^{18} cm^{-3} doping densities. The DOS function corresponding to this second subband rises much faster to unity (approaching the ideal DOS) when the surface-roughness scattering and Coulomb scattering is absent (third panel), compared to the case when only Coulomb scattering is absent (second panel). This can be attributed to the increased surface-roughness scattering that now dominates the inter-subband scattering, as previously stated.

The Coulomb scattering does not seem as significant in this case. This is also in accordance with our expectation that Coulomb scattering should dominate at lower energies which correspond to lower subbands. This is further asserted from the second panel data, which shows the increase of the slope in the DOS functions corresponding to the first subband from valley 1 and valley 2 when Coulomb scattering is absent.

V. Conclusions

We might conclude from the above analysis that collisional broadening of the states is more significant in smaller device structures with very high doping densities due to the Coulomb scattering being increased by two orders of magnitude and interface roughness dominating the intra-subband scattering in this structure at very high doping densities [16].

References

[1] T. Ando, A. B. Fowler and F. Stern, "Electronic Properties of Two-Dimensional Systems," Rev. Mod. Phys., Vol. 54, pp. 437-671, 1982.

[2] P. Hohenberg and W. Kohn, "Inhomogeneous Electron Gas," *Phys. Rev*., Vol 136, pp. B864-B871, 1964.

[3] W. Kohn and L. J. Sham, "Self-Consistent Equations Including Exchange and Correlation Effects," *Phys. Rev*., Vol 140, pp. A1133-A1140, 1965.

[4] L. V. Keldysh, "Diagram Technique for Nonequilibrium Processes," *Sov. Phys. JETP*, Vol. 20, pp. 1018-1026, 1965.

[5] L. P. Kadanoff and G. Baym, *Quantum Statistical Mechanics* (W. A. Benjamin, New York, 1992).

[6] J. Rammer and H. Smith, "Quantum Field-Theoretical Methods in Transport Theory of Metals," *Rev. Mod. Phys*., Vol. 58. pp. 323-359, 1986.

[7] D. K. Ferry and H. L. Grubin, "Modeling of Quantum Transport in Semiconductor Devices," *Solid St. Phys.,* Vol. 49, pp. 283-448 (Academic Press, New York, 1995).

[8] D. Vasileska and D. K. Ferry, "Scaled silicon MOSFET's: Part I - Universal mobility behavior", *IEEE Trans. Electron Devices*, Vol. 44, pp. 577-83, 1997.

[9] P. J. Price, "Two-Dimensional Electron Transport in Semiconductor Layers. I. Phonon Scattering," *Ann. Phys.*, vol. 133, pp. 217-239, 1981.

[10] B. K. Ridley, "Hot Electrons in Low-Dimensional Structures," *Rep. Prog. Phys.*, vol. 54, pp. 169-256, 1991.

[11] D. K. Ferry, "Hot-Electron Effects in Silicon Quantized Inversion Layers," *Phys. Rev. B*, vol. 14, pp. 5364-5371, 1976.

[12] T. Yamada, J.-R. Zhou, H. Miyata and D. K. Ferry, "In-Plane Transport Properties of $Si/Si_{1-x}Ge_x$ Structure and its FET Performance by Computer Simulation," *IEEE Trans. Electron Devices*, Vol. ED-41, pp. 1513-1522, 1994.

[13] D. K. Ferry, *Semiconductors* (Macmillan, New York, 1991).

[14] M. V. Fischetti and S. E. Laux, "Monte Carlo Study of Electron Transport in Silicon Inversion Layers," *Phys. Rev. B*, vol. 48, pp. 2244-2274, 1993.

[15] D. Vasileska, *Green's Functions Formalism for Low-Dimensional Systems*, PhD Thesis, Arizona State University, December 1995.

[16] G. D. Mahan, Many-Particle Physics (Kluwer Academic/Plenum Publishers, New York,2000).

[17] S. M. Goodnick *et al.*, "Surface roughness induced scattering and band tailing", *Surface Science* 113, 233 (1982).